

Reducing of Eu^{3+} Due to the Change of Topological Structure of BO_3 Unit in Borate Glass

Su Zhang,^a Ran Pang,^a Da Li,^a Jipeng Fu,^{a,b} Yonglei Jia,^{a,b} Haifeng Li,^{a,b} Wenzhi Sun,^{a,b} Lihong Jiang,^{*,a} and Chengyu Li^{*,a}

^aState Key Laboratory of Rare Earth Resources Utilization, Changchun Institute of Applied Chemistry, Chinese Academy of Sciences, Changchun 130022, P. R. China

^bUniversity of Chinese Academy of Sciences, Beijing 100049, P. R. China

1. Experimental

The composition of Eu^{2+} , Dy^{3+} co-doped strontium aluminoborate glass-ceramics was $45\text{B}_2\text{O}_3 \cdot 25\text{Al}_2\text{O}_3 \cdot 30\text{SrCO}_3 \cdot 0.05\text{Eu}_2\text{O}_3 \cdot 0.05\text{Dy}_2\text{O}_3$ (in mol%). Reagent-grade SrCO_3 , H_2BO_3 , Al_2O_3 , Eu_2O_3 and Dy_2O_3 were used as starting materials. Mixed batches were melted in alumina crucible at 1500 °C for 30 min under an ambient atmosphere. The crucible was covered by a lid to lower the evaporation of B_2O_3 . Then the liquid was poured onto a stainless steel plate that has been pre-heated in oven at 300°C and cooled to room temperature naturally.

XRD pattern was obtained on a Rigaku D/MAX-IIB x-ray diffractometer with $\text{Cu K}\alpha 1$ ($\lambda=1.5405 \text{ \AA}$) radiation. The measurements of photoluminescence (PL) and photoluminescence excitation (PLE) spectra were performed using a Hitachi F-7000 spectrometer equipped with a 150 W xenon lamp under a working voltage of 700 V. Fourier transform infrared (FT-IR) spectrum was measured with a BRUKER IFS66 v/s vacuum-type spectrometer with KBr pellet technique. Chromaticity coordinates and luminance were obtained with a Minolta CS-100A Chromameter. The quantum efficiency yield was analyzed with a PL quantum efficiency measurement system C9920-02 Hamamatsu Photonics, Shizuoka, Japan.

2. LLP Photographs of SABED

The photographs of SABED in Figure 1 were obtained with a digital camera Canon EOS-5D. Photograph in Figure 1 was taken under a Philips commercial fluorescence standard lamp (D65). The long-lasting phosphorescence image of SABED was taken when turn off the lamp. The chromaticity coordinates of the sample are $x=0.2842$, $y=0.5772$. The luminance is $3.53 \text{ cd}\cdot\text{m}^{-2}$, measured after the irradiation of fluorescent lamp with a power density of 12000 lx for 20 min. The limit of light perception for naked eyes is $0.32\times 10^{-3} \text{ cd}\cdot\text{m}^{-2}$, which means the LLP of the sample is quite strong.

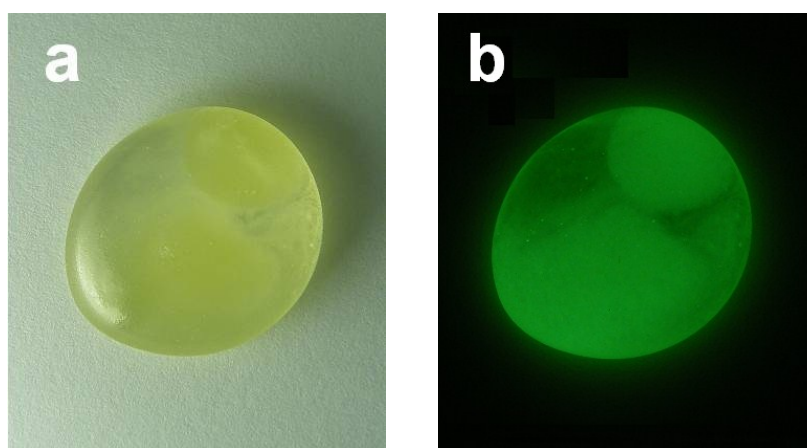


Figure S1 The photographs of SABED (a) for the sample exciting with a Philips commercial fluorescence lamp and (b) for the long-lasting phosphorescence image obtained in dark after the irradiation.

3. The emission and excitation spectra of SABED

Figure 2S shows the emission spectrum of SABED excited by 254nm. The spectrum behaves in a mixed emissions consisting of the band-emission of Eu^{2+} and line-emission of Eu^{3+} and Dy^{3+} . The 515nm band emission is ascribed to $4f^65d-4f^7(^8S_{7/2})$ transition of Eu^{2+} . The 486nm and 577nm peaked line-emissions are ascribed to the $^4F_{9/2}-^6H_{5/2}$ and $^4F_{9/2}-^6H_{13/2}$ transition of Dy^{3+} , and the line emission at 614 nm to the $^5D_0-^7F_2$ transition of Eu^{3+} ions. Compared with Figure 3 in the paper,

the red emission of Eu^{3+} is increased, because when excited at 254 nm the emission of Eu^{3+} is selectively excited.

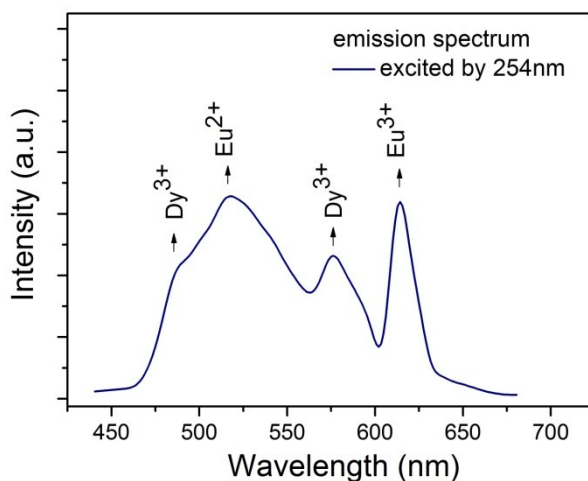


Figure 2S PL emission spectrum of SBAED excited by 254nm.

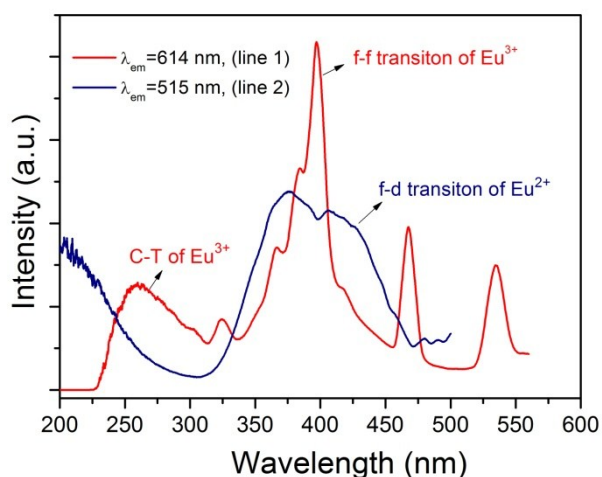


Figure 3S PL excitation spectrum of SBAED monitored at 614 (line 1) and 515 nm (line 2).

The PL excitation spectrum of SBAED is shown in Figure 3S. The two lines are totally different. Only a broad band was observed in line 2, which is due to the f-d transition of Eu^{2+} . Line 1, however, shows a complicate excitation peaks. The excitation band at about 255 nm is originated from the charge transfer between O and Eu^{3+} . The sharp lines in the 300–550nm range result from $4f-4f$ transitions of Eu^{3+} in the host, and the ${}^7F_0 \rightarrow {}^5L_6$ at 396nm and ${}^7F_0 \rightarrow {}^5D_2$ at 466 nm are two of the strongest

absorptions. Figure 3S means that there are no energy transfer between Eu^{2+} and Eu^{3+} . Actually, the Eu^{2+} and the Eu^{3+} ions are located in the different part of the glass sample. The Eu^{2+} ion is doped in the SrAl_2O_4 crystal and the Eu^{3+} ion is melted into the glass phase.

4. The site occupancy of Eu^{2+} in SrAl_2O_4

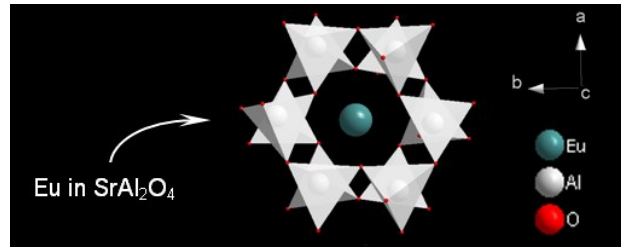


Figure 4S The site occupancy of Eu^{2+} in SrAl_2O_4 .

The crystal phase of SrAl_2O_4 adopts a stuffed tridymite monoclinic structure with space group of P21. Three pointing-up AlO_4 tetrahedra alternately connect three pointing-down AlO_4 tetrahedra by corner sharing to form a six-member ring. Six-member rings link to each other by a common oxygen of the pointing-up or -down tetrahedra to form the channels parallel to c-axis. These channels are further connected to form a 3-D framework by which each Eu^{2+} ion is effectively isolated and shielded from the oxidizing atmosphere and the neighboring Eu^{2+} ones.

5. The mechanism of LLP in $\text{SrAl}_2\text{O}_4:\text{Eu}^{2+}, \text{Dy}^{3+}$

$\text{SrAl}_2\text{O}_4:\text{Eu}^{2+}, \text{Dy}^{3+}$ is the famous commercial LLP material. Dy is the necessary codoped ion. By doping Dy, an appropriate crystal defect is formed. And interestingly, in a well synthesized Eu^{2+} and Dy^{3+} codoped SrAl_2O_4 sample, you will never find the emission of Dy^{3+} . Although there are some different mechanisms for the LLP, a common opinion is generally accepted. In the forbidden band of the SrAl_2O_4 crystal, some trap levels are existent, which may originated from the crystal defect such as oxygen vacancy (V_O), Sr vacancy (V_Sr), Dy_Sr^+ , etc. These traps can

capture and store the excitation energy, and then release it slowly at the thermal stimulation of room temperature giving the strong persistent luminescence called LLP (Chem. Mater. 2005, 17, 3904 and many other related references). LLP materials can be widely used in safety indication, detection of high-energy rays, road signs, automobile instruments, *in vivo* imaging and so on (Inorg. Chem. 2013, 52, 13875; Inorg. Chem. 2014, 53, 8638; Adv. Optical Mater. 2015 3 551; etc.).